

The energy-frequency diagram of the (1+1)-dimensional Φ^4 oscillon

N. V. Alexeeva,^a I. V. Barashenkov,^{b,1} Alain Dika,^{a,c} and Raphael De Sousa^a

^a*Department of Mathematics and Applied Mathematics, University of Cape Town, Rondebosch 7701, South Africa*

^b*Centre for Theoretical and Mathematical Physics, University of Cape Town, South Africa*

^c*Joint Institute for Nuclear Research, Dubna 141980, Russia*

E-mail: Nora.Alexeeva@uct.ac.za, Igor.Barashenkov@uct.ac.za,
A.Dika@uct.ac.za, dssrap001@myuct.ac.za

ABSTRACT: Two different methods are used to study the existence and stability of the (1+1)-dimensional Φ^4 oscillon. The variational technique approximates it by a periodic function with a set of adiabatically changing parameters. An alternative approach treats oscillons as standing waves in a finite-size box; these are sought as solutions of a boundary-value problem on a two-dimensional domain. The numerical analysis reveals that the standing wave's energy-frequency diagram is fragmented into disjoint segments with $\omega_{n+1} < \omega < \omega_n$, where $\omega_n = \omega_0/(n+1)$, $n = 0, 1, 2, \dots$, and ω_0 is the endpoint of the continuous spectrum (mass threshold of the model). The variational approximation involving the first, zeroth and second harmonic components provides an accurate description of the oscillon with the frequency in (ω_1, ω_0) , but breaks down as ω falls out of that interval.

¹Corresponding author.

Contents

1	Introduction	1
2	Multiscale variational approach	3
2.1	Method	3
2.2	Fixed points	5
2.3	Stability of the fixed point	7
3	Numerical standing waves	8
3.1	Energy-frequency diagram	8
3.2	Stability of standing waves	11
3.3	Standing waves vs oscillons	13
4	Numerical solution vs variational approximation	13
5	Concluding remarks	15
A	Appendix: Fixed points of the variational equations	16
B	Appendix: Linearisation matrix	19

1 Introduction

Oscillons (also known as pulsions) were introduced as localised long-lived pulsating structures in three-dimensional classical field theories [1–5]. The original motivation [6] was to model the vacuum domain formation in theories with spontaneous symmetry breaking and its cosmological implications. Oscillons have now been recognised to have a role in the dynamics of inflationary reheating, symmetry-breaking phase transitions, and false vacuum decay [5, 7–25]. They arise as natural ingredients in the bosonic sector of the standard model [26–30] and axion-based models of fuzzy dark matter [31–40]. The Einstein-Klein-Gordon equations have also been shown to exhibit oscillon solutions [41–47].

For some time, the studies of three-dimensional oscillons were disconnected from research into oscillatory solitons in 1D. The reason was that the latter objects — interpreted as the kink-antikink bound states [48–53] — were believed to persist over long periods of time (or even indefinitely), emitting little or no radiation. By contrast, the three-dimensional oscillons were thought to have a fairly short lifespan [2–5].

More accurate mathematical and numerical analysis indicated, however, that the oscillons in three dimensions and one-dimensional bound states share their basic properties [54–56]. (The only exception, of course, is the sine-Gordon breather — an exactly periodic solution which emits strictly no radiation.) It is for this reason that we are using the *oscillon*

nomenclature for what would otherwise be called “bion” [50, 57], “approximate breather” [58] or “breather-like state on the line” [59].

In this paper, we employ a new variational approach to study localised oscillations in the one-dimensional Φ^4 equation — the one-dimensional version of the system that bore the originally discovered pulsed states [1–3, 48, 49]. We consider our present attack on the one-dimensional Φ^4 oscillon a step towards the consistent variational description of its three-dimensional counterpart.

The 1+1 dimensional Φ^4 theory is probably the simplest model with spontaneous symmetry breaking exploited in the studies of quantum fields [60–67] and phase transitions [68, 69]. The model is defined by the Lagrangian

$$L = \frac{1}{2} \int [\Phi_t^2 - \Phi_x^2 - (\Phi^2 - 1)^2] dx \quad (1.1)$$

and equation of motion

$$\Phi_{tt} - \Phi_{xx} - 2\Phi(1 - \Phi^2) = 0. \quad (1.2)$$

Its oscillon solution was discovered by Dashen, Hasslacher and Neveu [49] who constructed it as an asymptotic series in powers of the amplitude of the oscillation. The first few terms in the expansion of [49] (with typos corrected) are

$$\begin{aligned} \Phi = & 1 + \frac{\epsilon}{\sqrt{3}} \operatorname{sech}(\epsilon x) \cos(\omega t) + \frac{\epsilon^2}{12} \operatorname{sech}^2(\epsilon x) [\cos(2\omega t) - 3] \\ & + \frac{\epsilon^3}{144\sqrt{3}} [98 \operatorname{sech}(\epsilon x) - 103 \operatorname{sech}^3(\epsilon x)] \cos(\omega t) + \frac{\epsilon^3}{48\sqrt{3}} \operatorname{sech}^3(\epsilon x) \cos(3\omega t) + O(\epsilon^4). \end{aligned} \quad (1.3)$$

Here $\omega^2 = \omega_0^2 - \epsilon^2$, $\epsilon \rightarrow 0$ and ω_0 denotes the mass of elementary constituents of the model (the endpoint of the continuous spectrum of vacuum excitations):

$$\omega_0 = 2.$$

Segur and Kruskal [58] proved that the series (1.3) does not converge and that the true oscillon expansion includes terms that are nonanalytic in ϵ . (For the system-dynamic perspective on this argument, see Eleonskii *et al* [70].) The nonanalytic terms lie beyond all orders of the perturbation theory and make negligible contributions to the core of the oscillon; yet they do not vanish as $|x| \rightarrow \infty$ and account for the oscillon-emitted radiation. Boyd [71] noted a close relationship between radiating (hence decaying) oscillons of small amplitude and *nanopterons*: standing waves with “wings” extending to the infinities. (See also [72].) The amplitude of the wings is exponentially small in ϵ but does not decrease as $x \rightarrow \pm\infty$. The sum of the standing wave and a solution to the linearised equation with an exponentially small amplitude gives a highly accurate approximation of the radiating oscillon [71].

Regarding oscillons of finite amplitude, numerical simulations have been the primary source of information. The earliest observations of oscillons with finite ϵ are due to Kudryavtsev [48], while more detailed and accurate sets of simulations can be found in [50, 52, 71, 72]. For reviews, see [56, 57, 73].

The present study is motivated by the need to have an analytic tool capable of providing insights into the structure and properties of the finite-amplitude oscillons, similar to the collective coordinate technique used in the nonlinear Schrödinger domain [74, 75]. Modelling on the multiscale variational method developed for the theory with the symmetric vacuum [76], we formulate a variational approach to the one-dimensional Φ^4 oscillon. The symmetry-breaking nature of the vacuum in (1.1) forces us to expand the set of collective coordinates that was employed in [76]. However, similar to [76], the expanded set does not include any radiation degrees of freedom. We approximate the oscillon by a strictly periodic, nonradiating, state.

To validate our variational approximation, we carry out a numerical study of the time-periodic solutions of equation (1.2) on a finite interval. The earlier studies determined standing waves with frequencies $\omega > \omega_0/\sqrt{2}$ [73]; we will reach below that record.

For each ω , there is a continuous family of standing waves with different amplitudes of the radiation wings and, consequently, different energies. We focus on the waves with the lowest energy as these nanopterons have the smallest wing amplitude [55, 56, 72]. The energy-frequency diagram of the lowest-energy standing waves is found to be in good agreement with the diagram constructed variationally in a wide range of frequencies.

The paper is organised into five sections. The variational approximation for the Φ^4 oscillons is presented in Section 2, with some technical details relegated to the Appendices. In Section 3, we determine numerical solutions describing standing waves in a finite-size box, and in Section 4, the results of the variational and numerical approaches are compared. Section 5 summarises conclusions of this study.

2 Multiscale variational approach

2.1 Method

The variational method is arguably the main analytical approach to solitons in nonintegrable systems outside the perturbation expansions. In the context of oscillons, the method was pioneered in Ref [5], where the three-dimensional Φ^4 oscillon was approximated by a localised waveform

$$\Phi = 1 + A(t)e^{-(r/b)^2}. \quad (2.1)$$

Here $A(t)$ is an unknown oscillatory function describing the trajectory of the structure's central point and b is an arbitrarily chosen value of its width. (Ref [77] followed a similar strategy when dealing with the two-dimensional sine-Gordon equation.) Once the ansatz (2.1) has been substituted in the lagrangian and the r -dependence integrated away, the variation of action produces a second-order equation for $A(t)$.

The regular variational method does not suggest any optimisation strategies for the choice of b . Making $b(t)$ another collective coordinate — as it is done in the studies of the nonlinear Schrödinger solitons [74, 75] — gives rise to an ill-posed dynamical system not amenable to numerical simulations [76, 78]. This difficulty is circumvented in the multiscale approach, which considers the oscillon as a rapidly oscillating structure with adiabatically changing parameters [76].

Following [76], we consider Φ to be a function of two time variables, $\mathcal{T}_0 = t$ and $\mathcal{T}_1 = \epsilon t$. The rate of change is assumed to be $O(1)$ on either scale: $\partial\Phi/\partial\mathcal{T}_0, \partial\Phi/\partial\mathcal{T}_1 \sim 1$. We require Φ to be periodic in \mathcal{T}_0 , with a period of T :

$$\Phi(\mathcal{T}_0 + T; \mathcal{T}_1) = \Phi(\mathcal{T}_0; \mathcal{T}_1).$$

As $\epsilon \rightarrow 0$, the variables \mathcal{T}_0 and \mathcal{T}_1 become independent and the Lagrangian (1.1) transforms into

$$L = \frac{1}{2} \int \left[\left(\frac{\partial\phi}{\partial\mathcal{T}_0} + \epsilon \frac{\partial\phi}{\partial\mathcal{T}_1} \right)^2 - \phi_x^2 - 4\phi^2 - 4\phi^3 - \phi^4 \right] dx, \quad (2.2)$$

where we let $\Phi = 1 + \phi$. The action $\int L dt$ is replaced with

$$S = \int_0^T d\mathcal{T}_0 \int d\mathcal{T}_1 L \left(\phi, \frac{\partial\phi}{\partial\mathcal{T}_0}, \frac{\partial\phi}{\partial\mathcal{T}_1} \right). \quad (2.3)$$

Modelling on the asymptotic expansion (1.3), we choose the trial function in the form

$$\phi = A \cos(\omega\mathcal{T}_0 + \theta) \operatorname{sech} \left(\frac{x}{b} \right) + [B + C \cos 2(\omega\mathcal{T}_0 + \theta)] \operatorname{sech}^2 \left(\frac{x}{b} \right), \quad (2.4)$$

where A, B, C, b and θ are functions of the ‘‘slow’’ time variable \mathcal{T}_1 while $\omega = 2\pi/T$ ($\omega > 0$).

Once the explicit dependence on x and \mathcal{T}_0 has been integrated away, equations (2.2) and (2.3) give

$$S = T \int d\mathcal{T}_1 \mathcal{L}_\omega, \quad (2.5)$$

where the effective Lagrangian \mathcal{L}_ω is given by

$$\mathcal{L}_\omega = K + \frac{b}{2} \left(A^2 + \frac{8C^2}{3} \right) (\dot{\theta} + \omega)^2 - U, \quad (2.6)$$

with

$$K = \frac{1}{2} \dot{A}(bA) + \frac{2}{3} \dot{B}(bB) + \frac{1}{3} \dot{C}(bC) + \frac{\dot{b}^2}{2b} \left[\left(\frac{\pi^2}{36} + \frac{1}{3} \right) A^2 + \frac{2\pi^2}{45} (2B^2 + C^2) \right] \quad (2.7)$$

and

$$\begin{aligned} U = & \left(\frac{1}{6b} + 2b \right) A^2 + \frac{4}{15} \left(\frac{1}{b} + 5b \right) (2B^2 + C^2) \\ & + 2b \left[\frac{8}{15} B(2B^2 + 3C^2) + A^2(2B + C) \right] \\ & + b \left[\frac{A^4}{4} + \frac{16}{35} \left(B^4 + \frac{3}{8} C^4 + 3B^2 C^2 \right) + \frac{4}{5} A^2 (2B^2 + C^2 + 2BC) \right]. \end{aligned} \quad (2.8)$$

In (2.7), we introduced a short-hand notation $\dot{f} \equiv \epsilon \partial f / \partial \mathcal{T}_1$.

The variation of the lagrangian (2.6) with respect to the collective coordinates A, B, C, b and θ produces five equations of motion. The variable θ is cyclic; the corresponding Euler-Lagrange equation gives rise to the conservation law

$$b \left(A^2 + \frac{8}{3} C^2 \right) (\dot{\theta} + \omega) = \ell, \quad (2.9)$$

where $\ell = \text{const}$. Making use of (2.9), $\dot{\theta}$ can be eliminated from the remaining four equations which become a system of four equations for four unknowns (A, B, C and b):

$$\begin{aligned} \ddot{A} + \frac{\ddot{b}}{2b}A + \frac{\dot{b}}{b}\dot{A} - \left(\frac{\pi^2}{36} + \frac{1}{3}\right) \left(\frac{\dot{b}}{b}\right)^2 A + \left(4 + \frac{1}{3b^2}\right) A - \frac{9\ell^2}{(3A^2 + 8C^2)^2} \frac{A}{b^2} \\ + 4A(2B + C) + A^3 + \frac{8}{5}A(2B^2 + 2BC + C^2) = 0, \end{aligned} \quad (2.10a)$$

$$\begin{aligned} \ddot{B} + \frac{\ddot{b}}{2b}B + \frac{\dot{b}}{b}\dot{B} - \frac{\pi^2}{15} \left(\frac{\dot{b}}{b}\right)^2 B + \frac{4}{5} \left(5 + \frac{1}{b^2}\right) B \\ + \frac{3}{5}(5A^2 + 8B^2 + 4C^2) + \frac{6}{5}A^2(2B + C) + \frac{24}{35}B(2B^2 + 3C^2) = 0, \end{aligned} \quad (2.10b)$$

$$\begin{aligned} \ddot{C} + \frac{\ddot{b}}{2b}C + \frac{\dot{b}}{b}\dot{C} - \frac{\pi^2}{15} \left(\frac{\dot{b}}{b}\right)^2 C + \frac{4}{5} \left(5 + \frac{1}{b^2}\right) C - \frac{36\ell^2}{(3A^2 + 8C^2)^2} \frac{C}{b^2} \\ + 3 \left(A^2 + \frac{16}{5}BC\right) + \frac{12}{5}A^2(B + C) + \frac{36}{35}(4B^2 + C^2)C = 0, \end{aligned} \quad (2.10c)$$

$$\begin{aligned} A\ddot{A} + \frac{4}{3}B\ddot{B} + \frac{2}{3}C\ddot{C} + \left[2\frac{\ddot{b}}{b} - \left(\frac{\dot{b}}{b}\right)^2\right] \left[\left(\frac{\pi^2}{36} + \frac{1}{3}\right) A^2 + \frac{2\pi^2}{45}(2B^2 + C^2)\right] \\ + 4\frac{\dot{b}}{b} \left[\left(\frac{\pi^2}{36} + \frac{1}{3}\right) A\dot{A} + \frac{2\pi^2}{45}(2B\dot{B} + C\dot{C})\right] - \frac{3}{3A^2 + 8C^2} \frac{\ell^2}{b^2} \\ + \left(4 - \frac{1}{3b^2}\right) A^2 + \frac{8}{15} \left(5 - \frac{1}{b^2}\right) (2B^2 + C^2) + 4A^2(2B + C) + \frac{32}{15}B(2B^2 + 3C^2) \\ + \frac{1}{2}A^4 + \frac{32}{35} \left(B^4 + \frac{3}{8}C^4 + 3B^2C^2\right) + \frac{8}{5}A^2(2B^2 + C^2 + 2BC) = 0. \end{aligned} \quad (2.10d)$$

The system of four equations has a Lagrangian

$$\mathcal{L}_\ell = K - U_\ell, \quad (2.11a)$$

with

$$U_\ell = U + \frac{\ell^2}{2b \left(A^2 + \frac{8}{3}C^2\right)}. \quad (2.11b)$$

Here K is as in (2.7) and U as in (2.8). Note that the frequency ω has disappeared from the system (2.10)-(2.11), along with $\dot{\theta}$. The role of the single parameter has been taken over by the quantity ℓ . We also note that equations (2.10) conserve energy:

$$H = K + U_\ell. \quad (2.12)$$

2.2 Fixed points

Stationary solutions of the system (2.10) are given by critical points of the function $U_\ell(A, B, C, b)$. The numerical analysis reveals that one such point, continuously dependent on ℓ , exists for

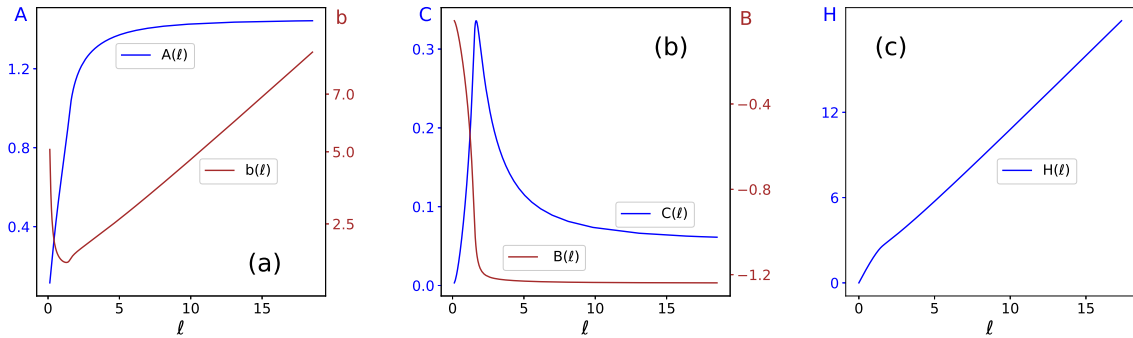


Figure 1. The fixed-point solutions of the variational equations (2.10). (a) amplitude of the first harmonic and width parameter; (b) amplitudes of the zeroth and second harmonic; (c) energy of the fixed point.

all $0 \leq \ell < \infty$ (see Appendix A). This nontrivial fixed point exists for the same reason why a classical particle moving in a centrally-symmetric confining potential has an equilibrium orbit with any nonzero angular momentum. The components of the fixed point are presented graphically in Fig 1(a-b). The energy of the stationary point,

$$H(\ell) = U_\ell [A(\ell), B(\ell), C(\ell), b(\ell)], \quad (2.13)$$

is shown in Fig 1(c).

It is worth mentioning here that our numerical continuation algorithm determines the components of the fixed point as functions of ω (rather than ℓ). Following the branch of fixed points that extends from $\omega_0 = 2$ to $\omega_c = 0.417\omega_0$ before reversing to $\omega_b = 0.527\omega_0$, we compute $\ell(\omega) = \omega b(A^2 + \frac{8}{3}C^2)$ (see Fig 7 in Appendix A). The functions $A(\ell)$, $B(\ell)$, $C(\ell)$, $b(\ell)$ and $H(\ell)$ in Fig 1 are then plotted as parametric curves. The asymptotic regime $\omega \rightarrow \omega_0$ corresponds to $\ell \rightarrow 0$; as the branch ω approaches its terminal point ω_b , we have $\ell \rightarrow \infty$.

Returning to the partial differential equation (1.2), the energy of its solutions is given by

$$E[\Phi] = \frac{1}{2} \int [\Phi_t^2 + \Phi_x^2 + (\Phi^2 - 1)^2] dx. \quad (2.14)$$

Substituting the ansatz (2.4) in the integral (2.14) gives a time-dependent quantity that cannot be used as a bifurcation measure of the trial function (2.4). However when the collective coordinates A, B, C and b take constant values, the integral (2.14) becomes periodic (with period T). In that case, we can define the *average* energy carried by the configuration (2.4):

$$\bar{E} = \frac{1}{T} \int_0^T E[\Phi] d\mathcal{T}_0. \quad (2.15)$$

Performing integration over \mathcal{T}_0 and x , equations (2.14) and (2.15) give $\bar{E} = U_\ell(A, B, C, b)$, where U_ℓ is as in (2.11b). Thus, the average field energy carried by the critical trial function

(that is, the function (2.4) with the parameters given by the fixed point $A(\ell), B(\ell), C(\ell), b(\ell)$) agrees with the energy integral of the variational equations (2.10) evaluated at that fixed point:

$$\overline{E}(\ell) = H(\ell) = U_\ell[A(\ell), B(\ell), C(\ell), b(\ell)]. \quad (2.16)$$

2.3 Stability of the fixed point

In order to classify the stability of the fixed points, it is sufficient to examine perturbations preserving the integral ℓ . Linearising equations (2.10) and assuming the time dependence of the form

$$(\delta A, \delta B, \delta C, \delta b)^T = e^{(\lambda/\epsilon)\mathcal{T}_1} \vec{y}, \quad (2.17)$$

where \vec{y} is a constant 4-vector, gives a generalised eigenvalue problem

$$M\vec{y} = -\lambda^2 P\vec{y}. \quad (2.18)$$

Here M and P are 4×4 symmetric real matrices. The M matrix is given in the Appendix B while

$$P = \begin{pmatrix} 2b & 0 & 0 & A \\ 0 & \frac{8}{3}b & 0 & \frac{4}{3}B \\ 0 & 0 & \frac{4}{3}b & \frac{2}{3}C \\ A & \frac{4}{3}B & \frac{2}{3}C & P_{44} \end{pmatrix}, \quad (2.19)$$

$$P_{44} = \pi^2 \frac{5A^2 + 16B^2 + 8C^2}{90b} + \frac{2}{3} \frac{A^2}{b}.$$

Note that the ansatz (2.17) tacitly assumes the exponents λ being of order ϵ .

The determinant of P is given by

$$\det P = \frac{32b^2}{405} [5(\pi^2 + 3)A^2 + 2(4\pi^2 - 15)(2B^2 + C^2)]. \quad (2.20)$$

Since $\det P > 0$, Sylvester's criterion implies that P is positive definite. Therefore, all generalised eigenvalues λ^2 are real and the exponents form pairs of real or pure imaginary opposite values, λ and $-\lambda$.

The generalised eigenvalues are computed numerically; the results are in Fig 2.

A negative eigenvalue emerges from the origin as ℓ is increased from zero. This is the only $O(\epsilon^2)$ eigenvalue present; all other generalised eigenvalues shown in Fig 2 (including three other ones occurring for small ℓ) are of order 1. Those large eigenvalues are inconsistent with the assumption underlying the ansatz (2.17); they do not carry any information on the stability properties of the oscillon. By contrast, the negative $O(\epsilon^2)$ eigenvalue appearing in the small- ℓ regime agrees with the stability of the Dashen-Hasslacher-Neveu's periodic solution in the limit $\omega \rightarrow \omega_0$ (where its slowly-varying amplitude satisfies the nonlinear Schrödinger equation.)

The absence of $O(\epsilon)$ exponents outside the asymptotic regime $\omega \rightarrow \omega_0$ implies that the oscillon remains stable as ω is reduced to lower values — for as long as our variational approximation remains valid. Indeed, had the instability set in at some $\omega_{\text{cr}} < \omega_0$, it would have brought along slowly-varying amplitude perturbations (of the periodic oscillation with the frequency ω_{cr}). The associated $O(\epsilon^2)$ eigenvalues would have been captured by the eigenvalue problem (2.18).

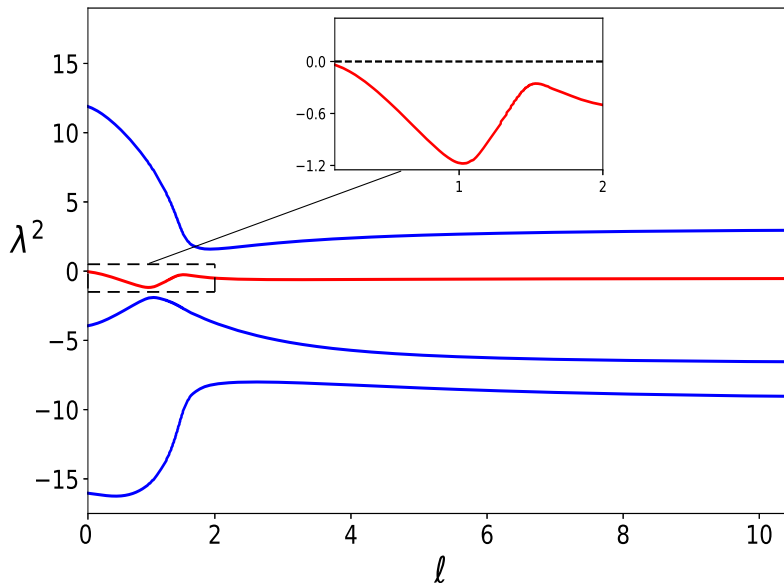


Figure 2. Roots of the characteristic equation $\det(M + \lambda^2 P) = 0$. The generalised eigenvalues λ^2 are shown as functions of ℓ . The blow-up of a segment of the branch emerging from the origin (plotted in red) highlights the fact that the eigenvalue never returns to zero.

3 Numerical standing waves

3.1 Energy-frequency diagram

To assess the accuracy of the variational approximation (2.4), we consider standing-wave solutions of the equation (1.2). The standing waves (also known as nanopterons [71] and quasibreathers [72]) are temporally periodic solutions assuming prescribed values at the ends of the finite interval $-R \leq x \leq R$. Confining the analysis to spatially symmetric (even) standing waves, we determine these as solutions of a boundary-value problem posed on a rectangular domain $(0, R) \times (0, T)$. Equation (1.2) with the boundary conditions

$$\Phi_x(0, t) = 0; \quad \Phi(R, t) = 1; \quad \Phi(x, 0) = \Phi(x, T) \quad (3.1)$$

was solved by a path-following algorithm with a Newtonian iteration. The half-length of the interval, R , was set to 40.

A typical solution consists of a localised core and a non-decaying small-amplitude wing, resulting from the interference of the outgoing radiation and radiation reflected by the boundary at $x = R$.

Fig 3 shows the energy

$$E_R[\Phi] = \int_0^R [\Phi_t^2 + \Phi_x^2 + (\Phi^2 - 1)^2] dx \quad (3.2)$$

of solutions of the boundary-value problem (1.2), (3.1). There are two features that attract attention in the figure.

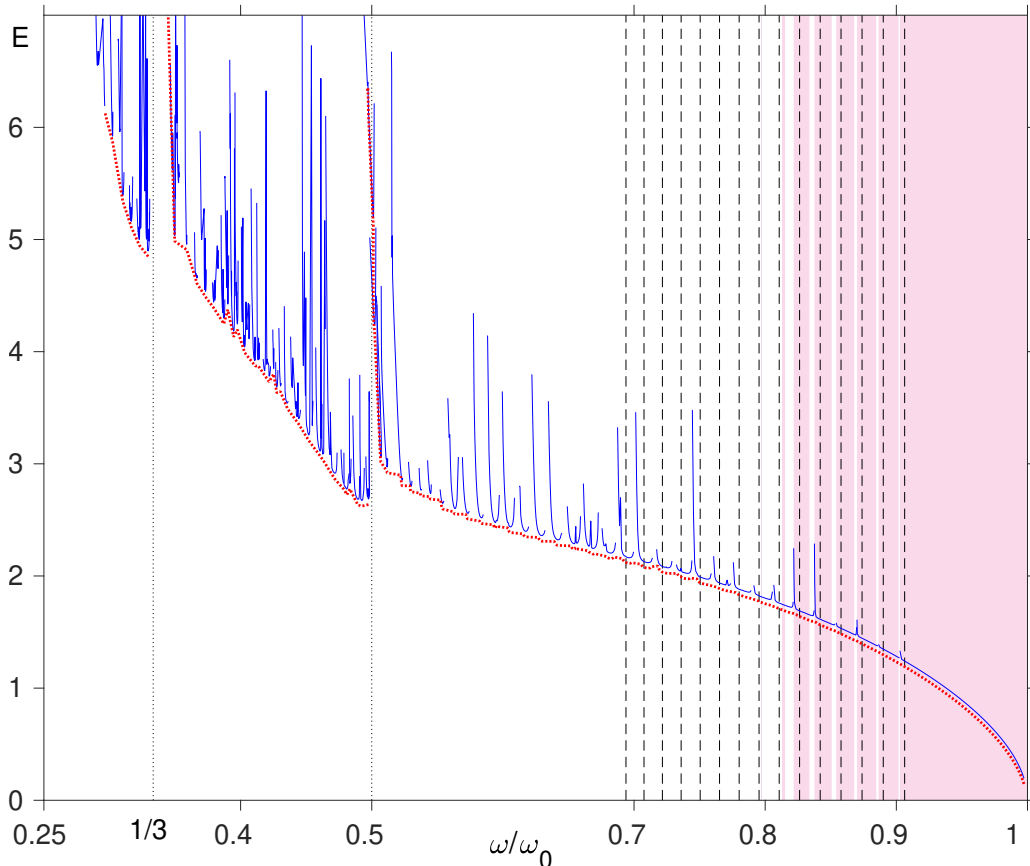


Figure 3. The energy (3.2) of the numerical standing-wave solution (blue). The vertical dashed lines are drawn at the subharmonic resonance frequencies $\omega = \Omega^{(n)}/2$, where $\Omega^{(n)}$ are the frequencies (3.4) of the linear waves. The red dotted arc underlying the numerical curve is the envelope of the family of spikes. (For visual clarity, it has been shifted down by a tiny amount from its actual position.) Clearly visible are discontinuities of the envelope at $\omega/\omega_0 = 1/2$ and $\omega/\omega_0 = 1/3$. The pink-tinted bands demarcate the frequency intervals where all Floquet multipliers lie on the unit circle.

First, the energy-frequency diagram exhibits what appears to be a sequence of spikes. On a closer examination, each “spike” turns out to consist of a pair of $E(\omega)$ branches rising steeply but not joining together. As the point $(\omega, E(\omega))$ climbs up the slope of a spike, the amplitude of the standing wave’s wing grows — this accounts for the rapid growth of the energy of the solution.

Each spike is produced by the resonance between an overtone of the frequency of the core of the standing wave and the eigenfrequency $\Omega^{(n)}$ of a linear mode with some n . The linear modes are given by

$$\Phi = 1 + \epsilon \sin(\Omega^{(n)}\mathcal{T}_0) \cos(\kappa^{(n)}x), \quad (3.3)$$

where

$$\Omega^{(n)} = \sqrt{\omega_0^2 + (\kappa^{(n)})^2}, \quad \kappa^{(n)} = \frac{\pi}{R} \left(n + \frac{1}{2} \right) \quad (n = 0, 1, 2, \dots). \quad (3.4)$$

(Similar resonances have been detected in the three-dimensional version of the Φ^4 model [79].) The positions of the $\frac{1}{2}$ undertones of the linear modes are marked by the vertical dashed lines in Fig 3. One can clearly see a correspondence between the positions of the “spikes” and the points $\omega = \Omega^{(n)}/2$ through which the vertical lines are drawn. (We only show the mode undertones in the right-hand portion of the diagram, where the spikes are thin and stay clear of each other.)

The positions of the spikes are sensitive to the choice of the interval half-length, R . Let ω be a fixed frequency with $\omega_0/2 < \omega < \omega_0$ and R_A an arbitrarily chosen half-length ($R_A \gg 1$). Denote k the wavenumber of the second-harmonic radiation, satisfying the dispersion relation

$$(n\omega)^2 = \omega_0^2 + k^2 \quad (3.5)$$

with $n = 2$. By tuning R to a suitably chosen value R_ω within the interval $(R_A, R_A + \pi/k)$, the amplitude of the “wing” can be minimized (yet not reduced to zero). The corresponding value of E_R gives the minimum energy of the family of standing waves with frequency ω : $E_{\min}(\omega) = E_{R_\omega}$. The graph of $E_{\min}(\omega)$ comprises segments of the $E_{R_A}(\omega)$ curve outside the neighbourhoods of the spikes, while the full, gapless, $E_{\min}(\omega)$ arc can be obtained as the envelope of the family of curves with R in $(R_A, R_A + \pi/k)$.

Another aspect of Fig 3 that is worth commenting on, concerns the fragmentation of the $E(\omega)$ curve into three disjoint branches with ω in the intervals $(\omega_*, \frac{1}{3}\omega_0)$, $(\frac{1}{3}\omega_0, \frac{1}{2}\omega_0)$ and $(\frac{1}{2}\omega_0, \omega_0)$, respectively. Here $\omega_* = 0.289\omega_0$ is the lowest frequency value for which we obtained a solution of the boundary-value problem (1.2), (3.1). The endpoints of the intervals, $\omega_0/2$ and $\omega_0/3$, are marked by a rapid growth of the energy E_{\min} as ω approaches these points from the right, and by finite energy jumps — as ω approaches these values from the left.

The fragmentation admits a simple explanation in terms of the dispersion relation (3.5). According to (3.5), the n -th harmonic radiation can only be emitted by the core oscillating with the frequency $\omega > \omega_0/n$. In the event of the coexistence of the n -th and $(n + 1)$ -th harmonics, the lower (the n -th) overtone will be energetically dominant. Therefore the radiation waves should be dominated by the fourth, third and second harmonic in the frequency ranges $(\frac{1}{4}\omega_0, \frac{1}{3}\omega_0)$, $(\frac{1}{3}\omega_0, \frac{1}{2}\omega_0)$ and $(\frac{1}{2}\omega_0, \omega_0)$, respectively. The harmonic waves forming the wings of our numerically obtained nanoopteron do comply with this selection rule.

Raising ω through $\omega_0/2$ opens a channel of the quadratic radiation — a more powerful channel than the $n = 3$ channel available to cores oscillating at $\omega < \omega_0/2$. The amplitude of the wing increases and this accounts for the energy jump in Fig 3. Similarly, the energy jump observed as ω is increased through $\omega_0/3$ is due to the opening of the third-harmonic channel, not accessible to the standing waves with $\omega < \omega_0/3$. We note that the energy jumps have the same origin as the staccato flashes of radiation from a slowly fading oscillon in the deformed sine-Gordon and ϕ^6 equations [80, 81].

As ω approaches $\omega_0/2$ from above, the wavenumber of the second-harmonic radiation tends to zero. The radiation wave transforms into a spatially uniform oscillation which acts as a parametric driver on the core of the standing wave. Since the frequency of the driver

is double that of the core, the parametric resonance condition is met and the amplitude of the core is boosted [82]. A similar argument explains the energy growth occurring as ω approaches $\omega_0/3$ from above.

3.2 Stability of standing waves

Let $\Phi_\omega(x, t)$ denote the solution of the boundary-value problem (1.2), (3.1) with $\omega = 2\pi/T$. To classify its stability, we linearise (1.2) about this solution:

$$y_{tt} - y_{xx} - 2y + 6\Phi_\omega^2(x, t)y = 0. \quad (3.6)$$

Equation (3.6) is supplemented with the boundary conditions

$$y_x(0, t) = y_x(R, t) = 0; \quad (3.7)$$

that is, we confine our study to perturbations sharing the symmetry of the standing wave and vanishing at the same point on the x -line.

Having expanded $y(x, t)$ in the cosine Fourier series in the interval $(0, R)$ and keeping only the first N harmonics, we have evaluated the monodromy matrix of the T -periodic solution for each ω in Fig 3. (We took $N = 512$.) If all eigenvalues μ_n ($n = 1, 2, \dots, 2N$) of the monodromy matrix satisfy $|\mu_n| = 1$, the periodic solution $\Phi_\omega(x, t)$ is deemed stable. If there are Floquet multipliers with $|\mu_n| > 1$, the standing wave Φ_ω is linearly unstable.

The frequency intervals with no multipliers outside the unit circle are indicated by pink bands in Fig 3. In particular, the entire region $0.903 < \frac{\omega}{\omega_0} < 1$ is found to be stable. As ω is continuously turned down from $0.903\omega_0$, a pair of real eigenvalues (μ_m and μ_m^{-1}) repeatedly emerge and return to the unit circle. (The intervals of ω characterised by the presence of $\mu_m > 1$ are left blank in Fig 3.) After the frequency has reached below $0.798\omega_0$, the off-circle pair remains in the Floquet spectrum for any further decrease of ω .

The instability occurring in parts of the range $\omega \gtrsim 0.75\omega_0$ is weak. (Here we are assuming that the solution is not on the slope of a resonant peak). Specifically, the growth rate $\lambda = \frac{1}{T} \ln \mu_m$ associated with the Floquet multiplier $\mu_m > 1$ is bounded by 3×10^{-3} . As ω is decreased below $0.75\omega_0$, the unstable real eigenvalue becomes larger. In addition, complex quadruplets $\{\mu, \mu^*, \frac{1}{\mu}, \frac{1}{\mu^*}\}$ emerge from the unit circle.

To understand the effect of instability, we solved equation (1.2) on the interval $(-R, R)$, with the initial conditions

$$\Phi(x, 0) = \Phi_\omega(x, 0), \quad \frac{d\Phi(x, 0)}{dt} = \frac{d\Phi_\omega(x, 0)}{dt}, \quad |x| \leq R \quad (3.8)$$

and boundary conditions $\Phi(\pm R, t) = 1$. The initial perturbation of the standing wave was introduced by the finite-difference approximation of the derivative $d\Phi_\omega(x, 0)/dt$ of the boundary-value problem (1.2), (3.1).

We examined the standing waves with a string of ω values from the interval $(0.45\omega_0, 0.90\omega_0)$. The growth of instability of an unstable nanopterion with $0.75\omega_0 < \omega < 0.90\omega_0$ was expectedly very slow; the structure had to perform hundreds or even thousands of oscillations before any change would become noticeable. Consequently, we classify the

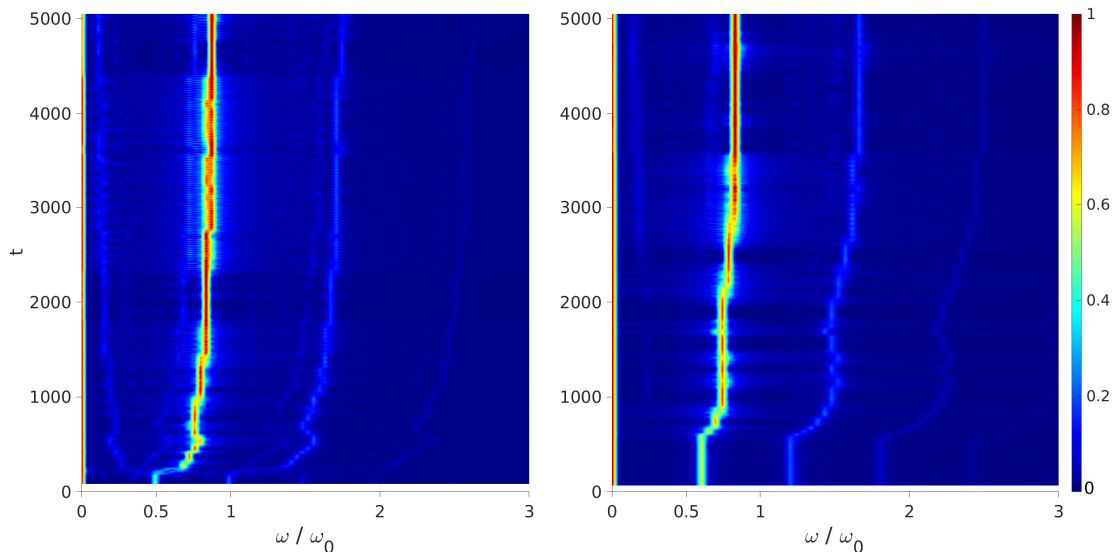


Figure 4. Spectral evolution of the core of the unstable standing wave. Colour encodes the (normalised) absolute value of the short-time Fourier transform $F(\omega, t) = \int_t^{t+\tau} e^{i\omega t'} \Phi(0, t') dt'$, where $\Phi(x, t)$ is the solution of the initial-value problem (1.2), (3.8) with $\omega = 0.4975\omega_0$ (a) and $\omega = 0.606\omega_0$ (b). In either case a rapid growth of the fundamental frequency of the oscillatory structure gives way to its slow drift along the $E_{\min}(\omega)$ curve. The width of the sliding window, τ , was set to 83 in (a) and 69 in (b).

standing-wave solutions in that interval as *practically stable* and turn to the complementary range.

When a nanopterion with the frequency in $(0.45\omega_0, 0.75\omega_0)$ had its energy close enough to the envelope value $E_{\min}(\omega)$ (that is, when we picked up a standing wave with the energy lying at the bottom of one of the lobes in Fig 3), the growing instability would not lead to the disintegration of the localised structure. It would just send the standing wave to the stable part of the $E_{\min}(\omega)$ curve (typically, to ω values near $0.85\omega_0$).

The transition would proceed in two stages. (See Fig 4.) The first stage involves a rapid growth of the fundamental frequency of the oscillatory structure, with its energy dropping under the envelope curve in Fig 3. The second part of its journey begins when the growing frequency brings the point $(\omega, E(\omega))$ back to the envelope curve (whose descent becomes steeper as ω grows). Once the structure has caught up with the $E_{\min}(\omega)$ curve, it will continue to lose energy — slowly sliding down that arc.

It is appropriate to note that there is no fundamental difference between the evolution of the unstable standing waves with ω on the left and on the right of the discontinuity at $\omega_0/2$ in Fig 3 (as long as ω does not fall under $0.45\omega_0$). (Compare Fig 4(a) to 4(b).) Furthermore, the instability growth is not accelerated as ω crosses through the critical value of $\omega_0/2$. Unlike the staccato transition reported in [80, 81], the instability does not depend on the availability of radiation channels.

We close this section with a remark on the standing waves with low frequencies, $\omega < 0.45\omega_0$. The instability takes violent forms in this range: a tiny perturbation breaks the standing wave into a kink-antikink pair or a pair of diverging oscillons. The analysis of these processes is left as a future challenge.

3.3 Standing waves vs oscillons

What do the standing waves in a box teach us about the behaviour of oscillons, the oscillatory radiating lumps on the endless line? To gain insight into the relation between the two types of objects, we simulated equation (1.2) with the initial condition of the form

$$\Phi(x, 0) = \Phi_\omega(x, 0), \quad \frac{d\Phi(x, 0)}{dt} = \frac{d\Phi_\omega(x, 0)}{dt}, \quad |x| \leq R; \quad (3.9)$$

$$\Phi(x, 0) = \frac{d\Phi(x, 0)}{dt} = 0, \quad R < |x| < \tilde{R}, \quad (3.10)$$

on an interval $(-\tilde{R}, \tilde{R})$, where $\tilde{R} \gg R$. (We took $\tilde{R} = 80$.) The radiation-absorbing pads placed near the endpoints of the interval emulated the infinite line situation.

In this “infinite space” experiment, a standing wave that had been classified as stable in the $-R < x < R$ box was observed to drift, adiabatically, down the $E_{\min}(\omega)$ curve in Fig 3. By contrast, an *unstable* nanopteron was seen to leave the curve for a short while, return to it at a higher frequency, and then start sliding down the arc — first due to the growth of instability and later, when it is already in the stable domain, due to the radiative energy losses.

Thus, the family of standing waves with a varied frequency in a long box provides the trajectory followed by an adiabatically fading oscillon in its phase space.

4 Numerical solution vs variational approximation

Fig 5 compares the energy of the standing wave with the average energy (2.16) carried by the critical trial function. (The latter is given by (2.4) where A, B, C and b are taken to be the components of the fixed-point solution of equations (2.10).) For further comparison, we have included the energy of the asymptotic solution (1.3),

$$E = \frac{4}{3}\epsilon + \frac{32}{81}\epsilon^3, \quad (4.1)$$

where $\epsilon = \sqrt{\omega_0^2 - \omega^2}$ and corrections higher than ϵ^3 have been disregarded.

In the frequency range $(0.6\omega_0, \omega_0)$, the variational result (2.16) provides a fairly accurate approximation of the envelope of the numerical $E(\omega)$ curve. Remarkably, the variational answer is much closer to $E_{\min}(\omega)$ than the asymptotic expansion (4.1).

As ω is reduced from $0.6\omega_0$ to $0.5\omega_0$, the variational $\bar{E}(\omega)$ dependence deviates from its numerical counterpart and once ω has fallen under $\omega_0/2$, the numerical-variational correspondence breaks down entirely. The envelope of the numerical curve in Figs 3 and 5 is split into three fragments, with E_{\min} growing monotonically as ω decreases within each fragment. There is a unique value of E_{\min} for each ω . By contrast, the variational energy

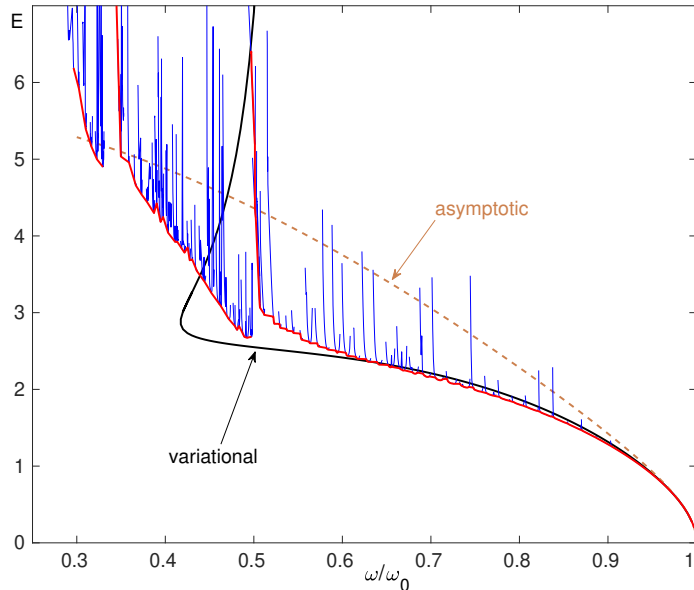


Figure 5. The energy (2.14) of the standing-wave solution determined numerically (blue), with the envelope curve plotted in red. (Unlike Fig 3, the envelope is shown in its true position here.) The black line depicts the average energy (2.16) carried by the trial function (2.4) with parameters given by the fixed-point of the variational equations. The dashed parabola indicates the asymptotic result (4.1).

$\bar{E}(\omega)$ grows as ω is reduced from ω_0 to $\omega_c = 0.417\omega_0$, but then the curve turns back so that there are two coexisting branches for each ω in the interval (ω_c, ω_b) , where $\omega_b = 0.527\omega_0$.

The stability of the standing wave with $\omega > 0.9\omega_0$ and its *practical* stability in the interval $0.75\omega_0 < \omega < 0.9\omega_0$ are reproduced by the variational approach. However the stability properties are not immune from the general deterioration of the variational approximation occurring as ω is reduced. Specifically, the numerical analysis reveals that the nanoopteron becomes unstable as ω falls under $0.75\omega_0$ whereas the variational method fails to capture this instability.

The numerical analysis suggests three factors that contribute to the failure of the variational approximation with low ω . First, the amplitude of the radiation emitted from the core of the wave (and reflected from the boundary at $x = R$) grows as its frequency is decreased. By contrast, the ansatz (2.4) does not take into account the radiation wing at all. Second, as ω is lowered below $\omega_0/2$, the contribution of the first harmonic to the Fourier spectrum of the core decreases while the role of higher harmonics grows. As a result, the variational ansatz (2.4) — which keeps $\cos(\omega\mathcal{T}_0 + \theta)$ but does not include $\cos 3(\omega\mathcal{T}_0 + \theta)$ — becomes inadequate. Finally, the spatial profile of the low-frequency nanoopteron’s core exhibits several humps and cannot be emulated by the bell-shaped ansatz (2.4).

5 Concluding remarks

A variational approach to a localised structure aims to identify the collective coordinates that capture the essentials of its dynamics. The choice of essential coordinates is validated by the agreement between the finite-dimensional description of the structure and its true properties as revealed by the numerical analysis. In this study, we utilised the multiscale variational method to determine the nonlinear modes responsible for the formation and stability of the one-dimensional ϕ^4 oscillons.

The method was previously applied [76] to oscillons of the Kosevich-Kovalev model [83], defined by the Lagrangian

$$L = \frac{1}{2} \int (\phi_t^2 - \phi_x^2 - 4\phi^2 + \phi^4) dx. \quad (5.1)$$

An ansatz comprising three variables,

$$\phi = A \cos(\omega \mathcal{T}_0 + \theta) \operatorname{sech}\left(\frac{x}{b}\right), \quad (5.2)$$

was found to provide an accurate agreement with the numerical simulations of the corresponding equation of motion.

The ϕ^4 Lagrangian of the present paper,

$$L = \frac{1}{2} \int (\phi_t^2 - \phi_x^2 - 4\phi^2 - 4\phi^3 - \phi^4) dx, \quad (5.3)$$

is different from (5.1) in the presence of the symmetry-breaking ϕ^3 term. This term would not contribute to the effective Lagrangian generated by the trial function (5.2); the single-harmonic ansatz is “blind” to the cubic term. To capture the asymmetry in oscillations, we have had to extend the single-harmonic ansatz (5.2) to a sum of three harmonics in (2.4). Accordingly, the number of collective variables has increased from three to five.

Our variational study was complemented by the numerical analysis of equation (1.2) on a periodic two-dimensional domain $(0, R) \times (0, T)$. Solutions of this boundary-value problem are standing waves consisting of a localised core and small-amplitude wings formed by the interference of the radiation emitted by the core and radiation reflected from the boundaries. We obtained solutions with all ω between $0.3\omega_0$ and ω_0 , where $\omega = 2\pi/T$ is the fundamental frequency of the wave and ω_0 is the endpoint of the continuous spectrum.

Results are summarised in Fig 3 which shows the energy of the standing wave as a function of its frequency. The diagram features a sequence of spikes generated by the resonant growth of the wing amplitude. The envelope of the family of $E_R(\omega)$ curves with varied R gives the energy curve of the standing wave with the thinnest wings. The envelope is found to be fragmented according to the dominant radiation harmonic (second, third, or higher).

Fig 5 attests to a good agreement between the numerical energy-frequency dependence and its variational counterpart $\overline{E}(\omega)$ in the interval $(0.6\omega_0, \omega_0)$. As ω is decreased below $0.6\omega_0$, the agreement deteriorates and then breaks down completely. While the energy of the numerical solution changes monotonically within each of the three fragments of its $E(\omega)$ diagram, the variational curve turns back into a coexisting branch of fixed points (Fig 5).

As for the stability properties of the standing wave and its finite-dimensional approximation, their interval of consistency is even shorter. The numerical standing wave loses its stability once ω has dropped below $0.75\omega_0$ whereas the fixed-point solution of the variational equations remains stable over its entire existence domain, $(0.417\omega_0, \omega_0)$.

Acknowledgments

We thank N Quintero for useful discussions. This research was supported by the NRF of South Africa (grant No SRUG2204285129). One of the authors (A.D.) gratefully acknowledges a visiting fellowship from the Joint Institute for Nuclear Research where this project was completed.

A Appendix: Fixed points of the variational equations

The fixed points of the dynamical system (2.10) satisfy four simultaneous algebraic equations

$$\frac{1}{3b^2} - 1 + A^2 + \frac{4}{5}C^2 + \frac{4}{5}\left(\frac{5}{2} + 2B + C\right)^2 = \omega^2, \quad (\text{A.1a})$$

$$\frac{1}{3}\left(5 + \frac{1}{b^2}\right)B + \frac{5}{4}A^2 + 2B^2 + C^2 + \frac{1}{2}A^2(2B + C) + \frac{2}{7}B(2B^2 + 3C^2) = 0, \quad (\text{A.1b})$$

$$\left(5 + \frac{1}{b^2}\right)C + \frac{15}{4}A^2 + 12BC + 3A^2(B + C) + \frac{9}{7}(4B^2 + C^2)C = 5\omega^2C, \quad (\text{A.1c})$$

$$\begin{aligned} & \frac{5}{8}\left(4 - \frac{1}{3b^2}\right)A^2 + \frac{1}{3}\left(5 - \frac{1}{b^2}\right)(2B^2 + C^2) + \frac{5}{2}A^2(2B + C) + \frac{4}{3}B(2B^2 + 3C^2) \\ & + \frac{5}{16}A^4 + \frac{1}{14}(8B^4 + 3C^4 + 24B^2C^2) + A^2(2B^2 + C^2 + 2BC) = \frac{5}{24}\omega^2(3A^2 + 8C^2). \end{aligned} \quad (\text{A.1d})$$

Note that we have switched from the parametrisation by ℓ back to the frequency ω , where

$$\omega = \frac{\ell}{b\left(A^2 + \frac{8}{3}C^2\right)}. \quad (\text{A.2})$$

While the invariant ℓ characterises the dynamics (in particular, stability) of solutions to equations (2.10), ω appears to be a more convenient parameter in the search for roots of (A.1).

Expressing A^2 from equation (A.1a) and substituting it in (A.1b), we obtain

$$b^{-2} = \frac{f_\omega(B, C)}{C + \frac{5}{2}} \quad (\text{A.3})$$

with

$$f_\omega = 10B + 12B^2 + 6C^2 + \frac{12}{7}B(2B^2 + 3C^2) + 3\left(\frac{5}{2} + 2B + C\right) \left[\omega^2 + 1 - \frac{4}{5}C^2 - \frac{4}{5}\left(\frac{5}{2} + 2B + C\right)^2 \right]. \quad (\text{A.4})$$

A similar substitution of A^2 in (A.1c) yields

$$b^{-2} = \frac{g_\omega(B, C)}{B + \frac{5}{4}} \quad (\text{A.5})$$

with

$$g_\omega = \frac{3}{2}(1 + \omega^2) \left(\frac{5}{2} + 2B - \frac{4}{3}C \right) + \left[10 + 12B + \frac{9}{7}(4B^2 + C^2) \right] C - \frac{6}{5} \left(\frac{5}{2} + 2B + 2C \right) \left[\left(\frac{5}{2} + 2B + C \right)^2 + C^2 \right], \quad (\text{A.6})$$

while eliminating A^2 between (A.1a) and (A.1d) produces

$$b^{-4} + p_\omega b^{-2} + q_\omega = 0, \quad (\text{A.7})$$

where

$$p_\omega(B, C) = 2 \left[\frac{16}{5} \left(B + \frac{5}{4} \right) \left(C + \frac{5}{2} \right) - \omega^2 - 6 \right] \quad (\text{A.8})$$

and

$$q_\omega(B, C) = 16 \left[2B^2 + (1 - \omega^2)C^2 + \frac{4}{5}B(2B^2 + 3C^2) + \frac{3}{70}(8B^4 + 3C^4 + 24B^2C^2) \right] - \frac{48}{25} \left[\left(\frac{5}{2} + 2B + C \right)^2 + C^2 - \frac{5}{4}(\omega^2 + 1) \right]^2. \quad (\text{A.9})$$

Before reducing the number of equations any further, it is fitting to note that the system (A.3), (A.5) and (A.7) has a root reproducing the asymptotic expansion (1.3):

$$B = -\frac{\epsilon^2}{4}, \quad C = \frac{\epsilon^2}{12}, \quad b^{-2} = \epsilon^2. \quad (\text{A.10})$$

Here we have defined a small parameter ϵ by letting, in equations (A.3), (A.5) and (A.7), $\omega^2 = 4 - \epsilon^2$. Using (A.1a) we recover the amplitude of the outstanding (first) harmonic in the Dashen-Hasslacher-Neveu's expansion:

$$A^2 = \frac{\epsilon^2}{3}. \quad (\text{A.11})$$

Returning to the system of three equations and using equation (A.3) to eliminate b^{-2} from (A.5) and (A.7), we arrive at

$$\left(B + \frac{5}{4} \right) f_\omega(B, C) - \left(C + \frac{10}{4} \right) g_\omega(B, C) = 0, \quad (\text{A.12a})$$

$$f_\omega^2(B, C) + \left(C + \frac{10}{4} \right) p_\omega(B, C) f_\omega(B, C) + \left(C + \frac{10}{4} \right)^2 q_\omega(B, C) = 0. \quad (\text{A.12b})$$

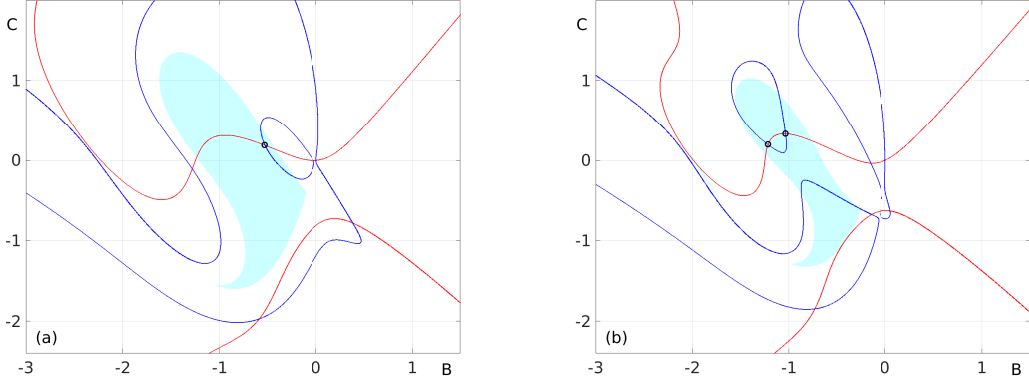


Figure 6. Graphical solution of the system (A.12) with $\omega = 0.71\omega_0$ (a) and $\omega = 0.45\omega_0$ (b). The red and blue curves are described by equations (A.12a) and (A.12b), respectively. Tinted in light blue is the “physical” region where the inequalities $A^2 > 0$ and $b^{-2} > 0$ are satisfied simultaneously, with A^2 and b^{-2} as in (A.13) and (A.3). Circles mark the roots of the system in the physical region.

For each ω , equations (A.12) with $f_\omega, g_\omega, p_\omega, q_\omega$ as in (A.4), (A.6), (A.8) and (A.9), comprise a system of two equations with two unknowns, B and C .

For much of the ω , the system (A.12) has multiple roots with real B and C (Fig 6). However only roots satisfying $A^2 > 0$ and $b^{-2} > 0$ correspond to fixed points of the variational equations (2.10). Here b^{-2} is given by (A.3) and A^2 by equation

$$A^2 = \frac{h_\omega(B, C)}{2C + 5} \quad (\text{A.13a})$$

with

$$h_\omega = -2B^2 - C^2 - B \left[\omega^2 + \frac{8}{3} + \frac{2}{7}(2B^2 + 3C^2) - \frac{4}{5}C^2 - \frac{4}{5} \left(\frac{5}{2} + 2B + C \right)^2 \right], \quad (\text{A.13b})$$

which ensues from (A.1a)-(A.1b).

There is only one such root when ω lies in the interval (ω_b, ω_0) , where $\omega_b = 0.527\omega_0$ (and $\omega_0 = 2$). In the vicinity of ω_0 , the corresponding fixed point is given by equations (A.10)-(A.11). The branch of fixed points extends from ω_0 to $\omega_c = 0.417\omega_0$ where it folds onto itself. As we path-follow the turning branch back to ω_b , the A, B and C components of the fixed point approach finite values while b grows without bound. As a result, the adiabatic invariant $\ell = \omega b(A^2 + \frac{8}{3}C^2)$ and the energy (2.13) tend to infinity as well (Fig 7).

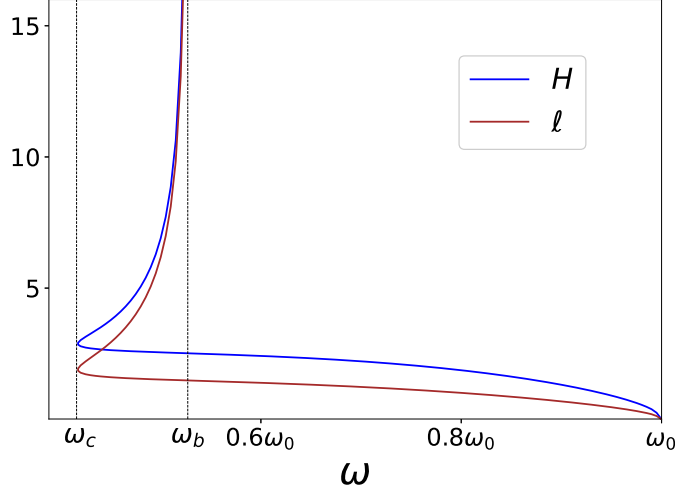


Figure 7. The adiabatic invariant ℓ and energy H of the fixed point as functions of ω .

B Appendix: Linearisation matrix

The matrix elements $M_{ij} = M_{ji}$ in equation (2.18) are given by

$$\begin{aligned}
M_{11} &= 24\omega^2 \frac{A^2 b}{3A^2 + 8C^2} + \frac{2}{3b} + 2b \left[3A^2 + \frac{4}{5} \left(\frac{5}{2} + 2B + C \right)^2 + \frac{4C^2}{5} - \omega^2 - 1 \right]; \\
M_{12} &= \frac{32}{5} Ab \left(\frac{5}{2} + 2B + C \right); \quad M_{13} = 64\omega^2 \frac{ACb}{3A^2 + 8C^2} + \frac{16}{5} Ab \left(\frac{5}{2} + 2B + 2C \right); \\
M_{14} &= 4\omega^2 A + \frac{8}{5} A \left(\frac{5}{2} + 2B + C \right)^2 + 2A \left(A^2 + \frac{4C^2}{5} - \frac{1}{3b^2} - \omega^2 - 1 \right); \\
M_{22} &= \frac{32}{5} A^2 b + \frac{32}{15b} + \frac{32}{105} b \left[36 \left(B + \frac{7}{6} \right)^2 + 18C^2 - 14 \right]; \quad M_{23} = \frac{16}{35} b (7A^2 + 24CB + 28C); \\
M_{24} &= \frac{16}{5} A^2 \left(\frac{5}{2} + 2B + C \right) + \frac{192}{35} \left(B + \frac{7}{6} \right) C^2 + \frac{8}{15} B \left[\frac{48}{7} \left(B + \frac{7}{4} \right)^2 - 1 \right] - \frac{32}{15} \frac{B}{b^2}; \\
M_{33} &= \frac{512}{3} \omega^2 \frac{C^2 b}{3A^2 + 8C^2} + \frac{192}{35} b \left(B + \frac{7}{6} \right)^2 + \frac{16}{15b} + \frac{16}{105} b (21A^2 + 27C^2 - 35\omega^2 - 14); \\
M_{34} &= \frac{32}{3} \omega^2 C + \frac{48}{35} C^3 + \frac{16}{15} \left[3A^2 + \frac{36}{7} \left(B + \frac{7}{6} \right)^2 - 5\omega^2 - 2 \right] C + \frac{16}{5} A^2 \left(B + \frac{5}{4} \right) - \frac{16}{15} \frac{C}{b^2}; \\
M_{44} &= \frac{2}{3} \frac{\omega^2}{b} (3A^2 + 8C^2) + \frac{2}{15b^3} (5A^2 + 16B^2 + 8C^2).
\end{aligned} \tag{B.1}$$

Here A, B, C and b are components of the real root of the system (A.1).

Note that the linearisation of equations (2.10) was carried out under the assumption that ℓ is a fixed, unperturbed, parameter: $\delta\ell = 0$. Also note that the frequency ω does

not appear in (2.10). However, once the linearisation procedure has been completed, we reintroduce ω according to

$$\omega = \frac{\ell}{b \left(A^2 + \frac{8}{3} C^2 \right)},$$

in agreement with (A.2). In the matrix elements (B.1), the variables A, B, C and b are single-valued functions of ℓ — and ω is also considered as a function of ℓ .

References

- [1] N A Voronov, I Y Kobzarev, and N B Konyukhova, Possibility of the existence of X mesons of a new type. JETP Lett **22** 290 (1975)
- [2] I L Bogolyubskii and V G Makhankov, On the pulsed soliton lifetime in two classical relativistic theory models. JETP Lett **24** 12 (1976)
- [3] I L Bogolyubskii and V G Makhankov, Dynamics of spherically symmetrical pulsions of large amplitude. JETP Lett **25** 107 (1977)
- [4] M Gleiser, Pseudostable bubbles. Phys Rev D **49** 2978 (1994)
- [5] E J Copeland, M Gleiser and H-R Müller, Oscillons: Resonant configurations during bubble collapse. Phys Rev D **52** 1920 (1995)
- [6] Ya. B. Zel'dovich, I. Yu. Kobzarev, and L. B. Okun'. Cosmological consequences of a spontaneous breakdown of a discrete symmetry. Sov. Phys.-JETP **40** 1 (1975)
- [7] A Riotto, Oscillons are not present during a first order electroweak phase transition. Phys Lett B **365** 64 (1996)
- [8] I. Dymnikova, L. Koziel, M. Khlopov, and S. Rubin, Quasilumps from first order phase transitions. Gravitation and Cosmology **6** 311 (2000)
- [9] M. Broadhead and J. McDonald, Simulations of the end of supersymmetric hybrid inflation and nontopological soliton formation. Phys. Rev. D **72** 043519 (2005)
- [10] M Gleiser, Oscillons in scalar field theories: applications in higher dimensions and inflation. Int. J. Mod. Phys. D **16** 219 (2007)
- [11] E. Farhi, N. Graham, A. H. Guth, N. Iqbal, R. R. Rosales, and N. Stamatopoulos, Emergence of oscillons in an expanding background. Phys. Rev. D **77** 085019 (2008)
- [12] M. Gleiser, B. Rogers, and J. Thorarinson, Bubbling the false vacuum away. Phys. Rev. D **77** 023513 (2008)
- [13] M. A. Amin, Inflaton fragmentation: Emergence of pseudo-stable inflaton lumps (oscillons) after inflation. arXiv:1006.3075 (2010)
- [14] M Gleiser, N Graham, and N Stamatopoulos, Generation of coherent structures after cosmic inflation. Phys Rev D **83** 096010 (2011)
- [15] M. A. Amin, R. Easther, H. Finkel, R. Flauger and M.P. Hertzberg, Oscillons after inflation. Phys. Rev. Lett. **108** 241302 (2012)
- [16] S-Y Zhou, E J Copeland, R Easther, H Finkel, Z-G.Moua and P M Saffin, Gravitational waves from oscillon preheating. JHEP **10** 026 (2013)
- [17] M Gleiser and N Graham, Transition to order after hilltop inflation. Phys Rev D **89** 083502 (2014)

- [18] P. Adshead, J. T. Giblin Jr., T. R. Scully and E. I. Sfakianakis, Gauge-preheating and the end of axion inflation. *Journ of Cosmology and Astroparticle Physics*, **12** 034 (2015)
- [19] J R Bond, J Braden and L Mersini-Houghton, Cosmic bubble and domain wall instabilities III: the role of oscillons in three-dimensional bubble collisions. *Journ Cosmology and Astroparticle Physics* **09** 004 (2015)
- [20] S Antusch, F. Cefalà and S Orani, Gravitational waves from oscillons after inflation. *Phys Rev Lett* **118** 011303 (2017)
- [21] J-P Hong, M Kawasaki, and M Yamazaki, Oscillons from pure natural inflation. *Phys Rev D* **98** 043531 (2018)
- [22] K. D. Lozanov and M. A. Amin, Gravitational perturbations from oscillons and transients after inflation. *Phys. Rev. D* **99** 123504 (2019)
- [23] D Cyncynates and T Giurgica-Tiron. Structure of the oscillon: The dynamics of attractive self-interaction. *Phys Rev D* **103** 116011 (2021)
- [24] K D Lozanov and V Takhistov. Enhanced Gravitational Waves from Inflaton Oscillons. *Phys. Rev. Lett.* **130** 181002 (2023)
- [25] J. C. Aurrekoetxea, K. Clough, and F. Muia. Oscillon formation during inflationary preheating with general relativity. *Phys. Rev. D* **108** 023501 (2023)
- [26] E. Farhi, N. Graham, V. Khemani, R. Markov, R. Rosales, An oscillon in the SU(2) gauged Higgs model. *Phys. Rev. D* **72** (2005) 101701(R);
- [27] N. Graham, An Electroweak Oscillon. *Phys. Rev. Lett.* **98** (2007) 101801; Numerical simulation of an electroweak oscillon. *Phys. Rev. D* **76** (2007) 085017;
- [28] M Gleiser, N Graham, and N Stamatopoulos, Long-lived time-dependent remnants during cosmological symmetry breaking: From inflation to the electroweak scale. *Phys Rev D* **82** 043517 (2010);
- [29] E. I. Sfakianakis, Analysis of oscillons in the SU(2) gauged Higgs model. arXiv:1210.7568 (2012)
- [30] M Piani and J Rubio. Preheating in Einstein-Cartan Higgs Inflation: oscillon formation. *JCAP* **12** 002 (2023)
- [31] E. W. Kolb and I. I. Tkachev, Nonlinear axion dynamics and the formation of cosmological pseudosolitons. *Phys. Rev. D* **49** 5040 (1994)
- [32] A Vaquero, J Redondo and J Stadler, Early seeds of axion miniclusters. *Journ of Cosmology and Astroparticle Physics* **04** 012 (2019)
- [33] M Kawasaki, W Nakanoa, and E Sonomoto, Oscillon of ultra-light axion-like particle. *Journ of Cosmology and Astroparticle Physics* **01** 047 (2020)
- [34] J Olle, O Pujolas, and F Rompineve, Oscillons and dark matter. *Journ of Cosmology and Astroparticle Physics* **02** 006 (2020)
- [35] A Arvanitaki, S Dimopoulos, M Galanis, L Lehner, J O Thompson, and K Van Tilburg, Large-misalignment mechanism for the formation of compact axion structures: Signatures from the QCD axion to fuzzy dark matter. *Phys Rev D* **101** 083014 (2020)
- [36] M Kawasaki, K Miyazaki, K Murai, H Nakatsuka, E Sonomoto, Anisotropies in cosmological 21 cm background by oscillons/ I-balls of ultra-light axion-like particle. *Journ of Cosmology and Astroparticle Physics* **08** 066 (2022)

- [37] S Antusch, F Cefalà, S Krippendorff, F Muia, S Orani and F Quevedo, Oscillons from string moduli. *JHEP* **01** 083 (2018)
- [38] Y Sang and Q-G Huang, Stochastic gravitational-wave background from axion-monodromy oscillons in string theory during preheating. *Phys. Rev. D* **100** 063516 (2019)
- [39] S Kasuya, M Kawasaki, F Otani, and E Sonomoto, Revisiting oscillon formation in the Kachru-Kalosh-Linde-Trivedi scenario. *Phys Rev D* **102** 043016 (2020)
- [40] K Imagawa, M Kawasaki, K Murai, H Nakatsuka and E Sonomoto. Free streaming length of axion-like particle after oscillon/ \mathcal{I} -ball decays. *JCAP* **02** 024 (2023)
- [41] V. A. Koutvitsky and E. M. Maslov, Gravipulsons. *Phys Rev D* **83** 124028 (2011); Passage of test particles through oscillating spherically symmetric dark matter configurations. *Phys Rev D* **104** 124046 (2021)
- [42] H-Y Zhang, Gravitational effects on oscillon lifetimes. *Journ of Cosmology and Astroparticle Physics* **03** 102 (2021)
- [43] Z Nazari, M Cicoli, K Clough and F Muia, Oscillon collapse to black holes. *Journ of Cosmology and Astroparticle Physics* **05** 027 (2021)
- [44] X-X Kou, C Tian and S-Y Zhou, Oscillon preheating in full general relativity. *Class. Quantum Grav.* **38** 045005 (2021)
- [45] T Hiramatsu, E I Sfakianakis and M Yamaguchi, Gravitational wave spectra from oscillon formation after inflation. *Journ High Energy Phys* **21** 2021 (2021)
- [46] X-X Kou, J B Mertens, C Tian and S-Y Zhou, Gravitational waves from fully general relativistic oscillon preheating. *Phys Rev D* **105** 123505 (2022)
- [47] K Nakayama, F Takahashia and M Yamada. Quantum decay of scalar and vector boson stars and oscillons into gravitons. *JCAP* **08** 058 (2023)
- [48] A E Kudryavtsev. Solitonlike solutions for a Higgs scalar field. *JETP Lett* **22** 82 (1975)
- [49] R F Dashen, B Hasslacher and A Neveu, Particle spectrum in model field theories from semiclassical functional integral techniques. *Phys Rev D* **11** 3424 (1975)
- [50] B S Getmanov. Bound states of solitons in the φ^4_2 field theory. *JETP Lett* **24** 291 (1976)
- [51] T. Sugiyama, Kink-Antikink collisions in the two-dimensional ϕ^4 model. *Prog. Theor. Phys.* **61**1550 (1979)
- [52] J Geicke. How stable are pulsons in the ϕ^4_2 field theory? *Phys Lett B* **133** 337 (1983)
- [53] D. K. Campbell, M.Peyrard. Solitary wave collisions revisited. *Physica D* **18** 47 (1986)
- [54] E P Honda and M W Choptuik, Fine structure of oscillons in the spherically symmetric φ^4 Klein-Gordon model. *Phys Rev D* **65** 084037 (2002)
- [55] G Fodor, P Forgács, P Grandclément, and I RÁCZ, Oscillons and quasibreathers in the ϕ^4 Klein-Gordon model. *Phys Rev D* **74** 124003 (2006)
- [56] G. Fodor. A review on radiation of oscillons and oscillatons. arXiv:1911.03340 [hep-th]
- [57] T I Belova, A E Kudryavtsev. Solitons and their interactions in classical field theory. *Physics - Uspekhi* **40** 359 (1997)
- [58] H Segur and M D Kruskal. Nonexistence of Small-Amplitude Breather Solutions in ϕ^4 Theory. *Phys Rev Lett* **58** 747 (1987)

- [59] S Dutta, D A Steer, T Vachaspati. Creating kinks from particles. *Phys Rev Lett* **101** 121601 (2008)
- [60] S. Rychkov and L. G. Vitale, Hamiltonian truncation study of the ϕ^4 theory in two dimensions. II. The \mathbb{Z}_2 -broken phase and the Chang duality, *Phys. Rev. D* **93**, 065014 (2016)
- [61] Z. Bajnok and M. Lajer, Truncated Hilbert space approach to the 2d ϕ^4 theory, *J. High Energy Phys.* **10** 050(2016)
- [62] M. Serone, G. Spada, and G. Villadoro, $\lambda\phi^4$ theory—Part II. The broken phase beyond NNNN(NNNN)LO, *J. High Energy Phys.* **05** 047 (2019)
- [63] M Bordag. Vacuum Energy for a Scalar Field With Self-Interaction in (1 + 1) Dimensions. *Universe* **7** 55 (2021)
- [64] N. Graham, H. Weigel. Quantum Corrections to Soliton Energies. *Int. J. Mod. Phys. A* **37** 2241004 (2022)
- [65] D. Szász-Schagrin and G. Takács. False vacuum decay in the (1 + 1)-dimensional φ^4 theory. *Phys Rev D* **106** 025008 (2022)
- [66] M A A Martin, R Schlesier, J Zahn. The semiclassical energy density of kinks and solitons. *Phys. Rev. D* **107** 065002 (2023)
- [67] H Ito, M Kitazawa. Gravitational form factors of a kink in 1+1 dimensional ϕ^4 model . *JHEP* **08** 033 (2023)
- [68] J Dziarmaga, P Laguma and W H Zurek. Symmetry Breaking with a Slant: Topological Defects after an Inhomogeneous Quench. *Phys Rev Lett* **82** 4749 (1999)
- [69] F Suzuki and W H Zurek. Topological defect formation in a phase transition with tunable order. *ArXiv:2312.01259 [cond-mat.stat-mech]*
- [70] V. M. Eleonskii, N. E. Kulagin, N. S. Novozhilova, and V. P. Silin. Asymptotic expansions and qualitative analysis of finite-dimensional models in nonlinear field theory. *Theor Math Phys* **60** 896 (1984)
- [71] J P Boyd. A numerical calculation of a weakly non-local solitary wave: the ϕ^4 breather. *Nonlinearity* **3** 177 (1990)
- [72] G Fodor, P Forgács, Z Horváth, and M Mezei. Computation of the radiation amplitude of oscillons. *Phys Rev D* **79** 065002 (2009)
- [73] J P Boyd. Continuum Breathers: Forty Years After. In: *A Dynamical Perspective on the ϕ^4 Model. Past, Present and Future*. P. G. Kevrekidis and J Cuevas-Maraver, Editors. *Nonlinear Systems and Complexity* vol. 26. Springer Nature, Switzerland (2019). <https://doi.org/10.1007/978-3-030-11839-6>
- [74] B A Malomed. Variational methods in nonlinear fiber optics and related fields. *Progress in Optics* **43** 71 (2002)
- [75] I V Barashenkov, N V Alexeeva, E V Zemlyanaya. Two- and three-dimensional oscillons in nonlinear Faraday resonance. *Phys Rev Lett* **89** 104101 (2002)
- [76] I V Barashenkov and N V Alexeeva. Variational formalism for the Klein-Gordon oscillon. *Phys Rev D* **108** 096022 (2023)
- [77] P. G. Kevrekidis, R. Carretero-González, J. Cuevas-Maraver, D. J. Frantzeskakis, J.-G. Caputo, B. A. Malomed. Breather stripes and radial breathers of the two-dimensional sine-Gordon equation. *Commun Nonlinear Sci Numer Simulat* **94** (2021) 105596

- [78] J G Caputo and N Flytzanis, Kink-antikink collisions in sine-Gordon and ϕ^4 models: Problems in the variational approach. *Phys Rev A* **44** 6219 (1991)
- [79] N V Alexeeva, I V Barashenkov, A. A. Bogolubskaya and E. V. Zemlyanaya. Understanding oscillons: Standing waves in a ball. *Phys Rev D* **107** 076023 (2023)
- [80] P. Dorey, T. Romańczukiewicz, Y. Shnir. Staccato radiation from the decay of large amplitude oscillons. *Phys Lett B* **806** 135497 (2020)
- [81] B. C. Nagy and G. Takacs. Collapse instability and staccato decay of oscillons in various dimensions. *Phys Rev D* **104** 056033 (2021)
- [82] I. V. Barashenkov, M. M. Bogdan and V. I. Korobov. Stability diagram of the phase-locked solitons in the parametrically driven damped nonlinear Schrödinger equation. *EPL* **15** 113 (1991)
- [83] A. M. Kosevich and A. S. Kovalev. Self-localization of vibrations in a one-dimensional anharmonic chain. *Sov Phys JETP* **40** 891 (1975)